Synergetic effects of NH$_3$ and NO$_X$ on the production and optical absorption of secondary organic aerosol formation from toluene photooxidation

Shijie Liu [a], Dandan Huang [b], Yiqian Wang [a], Si Zhang [a], Xiaodi Liu [a], Can Wu [a], Wei Du [a], Gehui Wang [a,c,*]

[a] Key Lab of Geographic Information Science of the Ministry of Education, School of Geographic Sciences, East China Normal University, Shanghai 210062, China

[b] State Environmental Protection Key Laboratory of Formation and Prevention of the Urban Air Pollution Complex, Shanghai Academy of Environmental Sciences, Shanghai 200233, China

[c] Institute of Eco-Chongming, Cuiniao Road, Chengjia Zheng, Shanghai 202150, China.

Corresponding author: Prof. Gehui Wang, e-mail: ghwang@geo.ecnu.edu.cn

Abstract

NH$_3$ is the most important alkaline gas in the atmosphere and one of the key species affecting the behaviors of atmospheric aerosols. However, the impact of NH$_3$ on secondary organic aerosol (SOA) formation remains poorly understood, especially the dynamic evolution of chemical compositions in the SOA formation process. In this study, a series of chamber experiments were performed to probe the individual and common effects of NH$_3$ and NO$_X$ on toluene SOA formation through OH-photooxidation. The chemical compositions of toluene SOA were characterized using the Aerodyne high-resolution time-of-flight aerosol mass spectrometer (AMS). The SOA yield increased from 28.1% in the absence of NH$_3$ to 34.7% in the presence of NH$_3$ but decreased to 19.5% in the presence of NO$_X$. However, the highest SOA yield of 42.7% and the lowest carbon oxidation state (OS$_C$) occurred in the presence of both NH$_3$ and NO$_X$, indicating that the higher volatility products that formed in the presence of NO$_X$ could partition into the particle-phase when NH$_3$ was added. This resulted in a synergetic effect on SOA formation when NH$_3$ and NO$_X$ co-existed. The heterogeneous reaction was the main pathway by which NH$_3$ participated in SOA formation in the photooxidation process. The synergetic effect of NH$_3$ and NO$_X$ was also observed in SOA optical absorption. A peak at 280 nm, which is characteristic of organonitrogen imidazole compounds, was observed in the presence of NH$_3$ and its intensity increased when NO$_X$ was added into the chamber. This work improves our understanding of how the synergistic interactions between NH$_3$ and NO$_X$ influence SOA formation and offers new insights into mitigating haze pollution.

44 **Keywords**: Photooxidation; Toluene; NH_3; Dynamic characteristics; Synergistic

45 effects

46

1 Introduction

Secondary organic aerosols (SOA) are an important component of atmospheric particulate matter (Moise et al., 2015;Liu et al., 2017), and can significantly affect atmospheric visibility, air quality, and human health (Paciga et al., 2014;Yang et al., 2016;Liu et al., 2017). Optical properties of SOA have been directly and indirectly linked to their effects on the climate (Laskin et al., 2015;Xie et al., 2017;Peng et al., 2020). Because of the complexity of their chemical components, oxidation processes, and environmental factors, SOA formation mechanisms are very complex and the current understanding of SOA formation is incomplete. This limited understanding hampers the ability of models to predict the magnitudes, dynamics, and distributions of atmospheric aerosols from particulate and precursor emissions (Ortiz-Montalvo et al., 2014). In the past decades, although our understanding of SOA formation mechanisms has been constantly improving, there is still a gap between the simulated SOA concentration in large-scale atmospheric models and field observations (Volkamer et al., 2006;Yang et al., 2018).

Ammonia (NH_3) is the most abundant and ubiquitous alkaline inorganic gas in the atmosphere and one of the critical factors influencing SOA formation (Wang et al., 2016;Wang et al., 2018b;Chen et al., 2019). Some studies have noted that the presence of NH_3 can contribute to the formation of more aerosol mass through photooxidation (Na et al., 2007;Li et al., 2018). Na et al. (2007) observed that aerosol yields in the α-pinene-ozone oxidation system increased by 8% when NH_3 was added. Li et al. (2018) reported that the presence of NH_3 in the aromatic hydrocarbon photooxidation system

69   increased aerosol size growth potentials (by 7%–108%), and resulted in enhanced SOA

70   formation. Qi et al. (2020) found that the concentration and average diameter of SOA

71   showed an immediate and rapid increase after adding NH_3. Furthermore, the acid-base

72   reactions between NH_3/NH_4^+ and the carboxyl groups in SOA molecules might enhance

73   SOA formation (Qi et al., 2020;Liu et al., 2015). The condensable ammonium salts

74   formed from the reaction between NH_3 and organic acids reduce the volatility of the

75   organic acids by several orders of magnitude (Paciga et al., 2014), and act as particle-

76   phase organics that further promote SOA formation (Na et al., 2007;Huang et al.,

77   2012;Chen et al., 2019;Qi et al., 2020;Wu et al., 2020). In addition, carbonyls can

78   undergo nucleophilic attack by NH_3 through the Maillard reactions and form the

79   corresponding iminium intermediates (Noziere et al., 2009;Laskin et al., 2015;Liu et

80   al., 2015). The iminium intermediates can continue to react with carbonyls, which

81   activates further transformations such as the formation of heterocyclic compounds and

82   oligomerization reactions and forms condensation (oligomeric) products with more

83   stable secondary imines (Schiff bases) (Laskin et al., 2014). Both Noziere et al. (2009)

84   and Ortiz-Montalvo et al. (2014) reported NH_3 is an efficient catalyst for reactions with

85   carbonyl compounds to form nitrogen-containing organic aerosols (NOA). The reaction

86   between carbonyl and NH_3 can significantly decrease the volatility of oxidation

87   products, which further increases the yield of SOA (Lee et al., 2013;Zhang et al.,

88   2015a;Qi et al., 2020). Babar et al. (2017) found that the substantial formation of

89   secondary imines in the presence of NH_3 was responsible for the higher α-pinene SOA

90   yields. However, not all studies have shown that the presence of NH_3 increases SOA

91   yields. One study observed that NH_3 suppressed SOA formation under certain

92   ozonation conditions (Ma et al., 2018b). Furthermore, the consumption of NH_3 by

93   Criegee intermediates was reported to decrease the secondary ozonide yield and thus

94   affect SOA formation.

95   Nitrogen oxides (NO_X = NO + NO_2), which are mainly emitted from the

96   combustion of fossil-fuels, have received significant attention due to their effects on the

97   photooxidation process of volatile organic compounds (VOCs) and SOA formation

98   (Surratt et al., 2006;Ng et al., 2007b;Draper et al., 2015;Berkemeier et al.,

99   2016;Sarrafzadeh et al., 2016;Zhao et al., 2018). A clear increase at first and then a

100   decrease in the SOA yield was found with increasing NO_X concentration from the

101   laboratory experiments with both anthropogenic (trimethylbenzene) and biogenic (β-

102   pinene) VOCs (Sarrafzadeh et al., 2016;Yang et al., 2020). The competitive chemistry

103   of organic peroxyl radicals (RO_2) with hydroperoxyl radicals (HO_2) and NO was

104   responsible for the variability in SOA formation (Ng et al., 2007a;Xu et al., 2014;Jiang

105   et al., 2020). RO_2 mainly reacts with HO_2 under low-NO_X conditions to form oxidation

106   products with lower volatility, which may enable it to partition into the particle-phase

107   and contribute to the SOA mass (Ng et al., 2007a). While the RO_2 + NO reaction is

108   dominant in high-NO_X conditions, the increase in volatile products formed through

109   fragmentation was responsible for the decrease in SOA yield with increasing NO_X

110   (Zhao et al., 2018;Liu et al., 2019a;Xu et al., 2020). In addition, the increase of OH

111   concentration formed through NO + $HO_2 \rightarrow NO_2$ + OH reaction at low-NO_X conditions,

112   and a suppressing effect of NO_X on OH formation under high-NO_X conditions was

113   partly responsible for the first increasing and then decreasing trend of SOA yield with

114   NO_X concentration (Sarrafzadeh et al., 2016;Bates et al., 2021).

115   In the last decade, atmospheric pollutants in China have changed significantly in

116   their concentrations and composition (Wang et al., 2015;Xia et al., 2016) with the

117   emissions of SO_2 and NO_X decreased by 75% from 2007–2015 and 10% from 2011–

118   2015, respectively (de Foy et al., 2016;Vu et al., 2019;Wang et al., 2020). However,

119   owing to the lack of regulation regarding NH_3 emissions, NH_3 emissions increased by

120   ~30 % from 2008–2016 over the North China Plain (Liu et al., 2018). As has been

121   pointed out in previous research, the promoting effect of NH_3 on the formation of SOA

122   may counteract the decreases in aerosol formation due to reductions in SO_2 and NO_X

123   (Zhang et al., 2021a). Indeed, field observation and model simulation have pointed out

124   that the simultaneous control of NH_3 emissions in conjunction with SO_2 emission is

125   more effective in reducing $PM_{2.5}$ than the process without NH_3 emissions control, and

126   $PM_{2.5}$ concentration can be more effectively reduced if NH_3 emission is decreased as

127   much as that of SO_2 (Erisman and Schaap, 2004). Hence, the mechanism by which NH_3

128   affects SOA formation has attracted more and more attention (Wang et al., 2018a;Ge et

129   al., 2019;Zhang et al., 2021b). However, previous studies have not paid sufficient

130   attention to the joint impacts of NH_3 and NO_X on the formation of SOA and its

131   corresponding optical properties. Due to the lack of real time detection methods for

132   SOA chemical composition, the dynamic characteristics of how NH_3 participates in

133   SOA formation via photooxidation have not been extensively studied.

134   Toluene is one of the most abundant aromatic VOCs in the urban atmosphere,

which is also an important source of brown carbon (Laskin et al., 2010;Ma et al., 2018a). The effects of NH_3 and NO_X on SOA formation through the toluene photooxidation process were investigated in this study. The chemical composition of toluene SOA was characterized on-line with an aerosol mass spectrometer and the characteristics of SOA chemical composition under different conditions were further explored by applying a positive matrix factorization (PMF) analysis. The optical properties of toluene SOA particles were determined based on a UV-vis spectrum analysis. Possible mechanisms of the effects of both NH_3 and NO_X on SOA formation were discussed. The results will help us to better understand SOA formation mechanisms under complex pollution conditions with elevated NH_3 and NO_X concentrations in an urban atmospheric environment.

2 Materials and Methods

2.1 Photooxidation chamber experiments

All toluene photooxidation experiments were performed in a 4 m^3 chamber. The chamber has been described in detail in our previous study (Liu et al., 2021). Briefly, the chamber was constructed with a 0.08 mm-thick FEP-Teflon film. 50 UV-B lamps (TUV36W, Philips) with peak wavelengths of 254 nm were set up around the chamber and used as the light source to drive OH radical formation through hydrogen peroxide (H_2O_2) photolysis. Mirror surfaced stainless steel was used as the interior wall of the enclosure to maximize and homogenize the interior light intensity. All experiments

155   were performed at room temperature (293~298 K) and atmospheric pressure was

156   maintained in the chamber at all times.

157   Before each experiment, the chamber was flushed with zero air for at least 18 hours,

158   after which the concentration of particles was less than 1 cm^{-3}. Zero air was generated

159   by a zero air supply (111-D3N, Thermo Scientific^{TM}, USA). The flow rate of zero air

160   was controlled at 20 L min^{-1} by a mass flow controller (D088C/ZM, Beijing Sevenstar

161   Electron Corporation) during the process of chamber reaction bag inflating. The relative

162   humidity (RH) of zero air was about 20%. For each experiment, measured amounts of

163   toluene (Sigma-Aldrich, analytically pure) and H_2O_2 solution (Sigma-Aldrich, 30 wt%

164   in H_2O) were injected into a Teflon bulb with micro syringes. Zero air was passed

165   through the injection tube to make sure all the liquids had evaporated to the gas-phase

166   and were blown into the chamber. Toluene concentration was measured with a Proton

167   Transfer Reaction-Mass Spectrometry (PTR-ToF-MS, Ionicon Analytik, Austria). The

168   evolution of toluene concentration for different experiments was shown in Fig. S1. The

169   OH concentration in the chamber was calculated based on the first order decay of

170   toluene concentration. There was no obvious difference of OH concentrations in the

171   different NO_X and NH_3 levels (Fig. S2). The average OH concentration over the entire

172   reaction period was 5.87 $\times$ 10^7 molecule cm^{-3}. NO_X (Air Liquid Shanghai, 510 ppm

173   NO_2 in N_2) and/or NH_3 (Air Liquid Shanghai, 502 ppm NH_3 in N_2) were introduced

174   directly into the chamber to reach the required concentrations. For experiments with

175   NO_X, although only NO_2 was introduced into the chamber before photooxidation, NO

176   could be formed through NO_2 photolysis under the UV light irradiation, so NO always

177 coexisted with NO_2 in the photooxidation system (Zhao et al., 2018). NOx

178 concentration was measured online by the NO-NO_2-NOx analyzer (Model 42C,

179 Thermo Electron Corporation, USA). Each experiment was performed without seed

180 aerosols. After all the reactants were added, the chamber stood quietly for 10 min

181 without turning on the light to ensure that the reactant gases in the chamber were evenly

182 mixed. The photooxidation started when the UV light was turn on.

183   The experimental conditions for the toluene photooxidation are listed in Table 1.

184 In our work, the OH and toluene concentrations were higher than those of urban

185 conditions. The purpose of the high OH and toluene concentrations is to obtain enough

186 particle production samples for off-line collections and accurate measurements. The

187 toluene concentrations remained stable under the different experimental conditions, the

188 variations of toluene-derived SOA mass concentration and yield were only affected by

189 the different NO_2 and/or NH_3 concentrations in this study. Toluene was studied here as

190 the representative of total aromatic VOCs in the urban atmosphere, thus its

191 concentration used in this study was much higher than that in the real atmosphere.

192 However, the concentration ratio of toluene to OH in this study is similar to that under

193 the real atmospheric conditions (Prinn et al., 1995;Zou et al., 2015).

194 **2.2 Particle concentration measurements**

195   For each experiment, a scanning mobility particle sizer (SMPS) was used to record

196 the particle size distribution and volume concentration of the toluene-derived SOA. The

197 SMPS was composed of a differential mobility analyzer (DMA model 3081, TSI Inc.,

198   USA) and a condensation particle counter (CPC model 3776, TSI Inc., USA) which

199   were used for screening particles with specific electrical mobility diameter (from 14.1

200   nm to 736.5 nm) and for counting the number of the selected particles, respectively.

201   The sheath gas velocity was 3 L min^{-1} and the sample gas velocity was 0.3 L min^{-1}. The

202   size scan was repeated every 5 min. During each scan circle, the scan time was 240 s,

203   and the particle sizes ranged from 13.6 nm to 726.5 nm. A density of 1.4 g m^{-3}, which

204   was measured by Ng et al. (2007), was used for the calculation of toluene SOA mass

205   concentration from the particle volume concentration (Ng et al., 2007b).

206   2.3 Chemical characterization

207   In this study, the toluene SOA chemical compositions were characterized with an

208   on-line high-resolution time-of-flight aerosol mass spectrometer (HR-ToF-AMS,

209   Aerodyne Research Inc. USA). The sample flow passed through a Nafion dryer and the

210   RH of the sample gas was reduced to below 20% before entering the AMS. In the

211   injection port, an aerodynamic lens focused particles with a vacuum aerodynamic

212   diameter below 1 μm into a narrow beam. Particles impacted a flash vaporizer (600°C)

213   at the rear of the sizing region under high vacuum (~10^{-7} Torr) and were subsequently

214   ionized by electron impact ionization (70 eV). Then, the positively charged ions entered

215   the ToF section and were separated. V-mode (m/Δm = ~2000) was used in the AMS

216   ToF section to achieve the high signal-to-noise ratio. The separated ion fragments were

217   analyzed by a mass spectrometer with scans from 1 to 300 m/z. The composition-

218   dependent collection efficiency (CE) was applied to the data based on the methods

219   established by Middlebrook et al. (2012). For mass concentration calculations, 1.1, 1.2,

220   and 1.4 were applied as the default relative ionization efficiency (RIE) values of nitrate,

221   sulfate, and organic compounds, respectively. The standard AMS data analysis software

222   SQUIRREL 1.63B coupled with PIKA 1.23B in the Igor Pro (WaveMetrics, Inc.,

223   Portland, Oregon), which were retrieved from http://cires1.colorado.edu/jimenez-

224   group/ToFAMSResources/ToFSoftware/, were used for the analysis of elemental ratios

225   and the ion speciated compositions of toluene SOA in the chamber. Note that the

226   elemental ratios (i.e., O/C, H/C, and N/C) and mass-to-carbon ratio (OM/OC) were all

227   calculated using the Aiken-Ambient method for comparability with previous studies

228   (Aiken et al., 2008). In order to further explore the changes in SOA chemical

229   composition, a PMF of the high-resolution mass spectra was performed to determine

230   the different organic aerosol (OA) factors during the toluene photooxidation process.

231   We preformed the PMF analysis in the same way as Zhang et al. (2011), the details of

232   which are provided in the Supporting Information.

233   **2.4 Absorption measurements**

234   The changes of absorption spectra and the absorbance of the toluene derived SOA

235   under different conditions were determined using a UV spectrophotometer (UV-3600,

236   Shimadzu, Japan) with a 1 cm cuvette. The SOA was collected from a 3 m^3 sample gas

237   onto the 46.2 mm PTFE filter (Whatman^{TM}, UK). The collected SOA sample was

238   dissolved in 5 mL of methanol (HPLC grade, > 99.8%) with 30 min of sonication. As

239   reported by Chen and Bond (2010), > 92 % of SOA is extractable by organic solvents

240 (e.g., methanol), which means that almost all organic matter was extracted in this study.

241 The filter extracts were filtered through 0.2 μm PTFE syringe filters to remove

242 suspended insoluble particles. Before detection of the optical absorbance, a cuvette

243 filled with pure methanol was scanned as a blank to provide a spectral background. The

244 absorption was detected over the range of 200 to 800 nm with a resolution of 0.5 nm^{-1}.

245 The light absorption coefficient of the particles at a specific wavelength λ (Abs_λ, M/m)

246 was calculated according to Eq. R1:

$$Abs_\lambda = (A_\lambda - A_{700}) \cdot \frac{V_l}{V_a \cdot L} \cdot \ln(10) \tag{R1}$$

247 where, A_{700} is the background value of light absorption intensity, calculated as the

248 average value of light absorption intensity from 695–705 nm to reduce the limits of

249 error in measurement; V_l and V_a are the volumes of methanol with dissolved particles

250 and sampled air, respectively; and L is the optical path length. Because Abs_λ was

251 strongly dependent on the amount of SOA, all Abs_λ results were normalized based on

252 the SOA mass collected on the filter. The normalized result was defined as the mass

253 absorption coefficient (MAC, $m^2\ g^{-1}$), calculated using Eq. R2:

$$MAC_\lambda = \frac{Abs_\lambda}{M} \tag{R2}$$

254 where, M ($\mu g\ m^{-3}$) represents the concentration of methanol-soluble organic carbon.

3 Result and Discussion

3.1 SOA formation

257 In order to investigate the effect of NH_3 and NO_X on SOA formation from toluene

258 photooxidation, a control test was carried out. SOA yield (Y) is defined as Y =

259     $\Delta M_0/\Delta HC$, where ΔM_0 is the produced organic aerosol mass concentration ($\mu g \ m^{-3}$),

260   and ΔHC is the mass concentration of reacted toluene ($\mu g \ m^{-3}$). The evolution of SOA

261   mass concentrations and SOA yield at different conditions during the photooxidation

262   process were shown in Fig. 1. Recent experiments showed that the wall loss of organic

263   vapors to the Teflon walls should not be ignored (Zhang et al., 2014;Zhang et al.,

264   2015b), and represented a major challenge in investigating SOA formation with

265   environmental chambers (Krechmer et al., 2020). The formation of SOA in laboratory

266   chambers may be substantially suppressed due to losses of SOA-forming vapors to

267   chamber walls, but this effect on SOA formation have not yet been quantitatively

268   established. However, the particle wall loss rates were detected at the end of the

269   chamber experiment after the UV-lamps were turned off, and the mass concentration

270   was corrected with the same way of Jiang et al. (2020) and Pathak et al. (2007). After

271   the wall loss correction, the particle mass concentration was almost constant, the

272   different wall loss effect caused by gaseous oxidation products formed in the different

273   experiment conditions was considered remedied. There was a noticeable increase in the

274   SOA mass concentration in the presence of NH_3, which was consistent with previous

275   studies (Qi et al., 2020;Chu et al., 2016). The mass concentration of SOA increased

276   from $637 \pm 14.6 \ \mu g \ m^{-3}$ without NH_3 to a maximum of $867 \pm 12.7 \ \mu g \ m^{-3}$ with 200 ppb

277   NH_3. Previous studies attributed the enhancement of SOA to the formation of NOA

278   from acid-base reactions between NH_3/NH_4^+ and carboxyl groups, or Maillard reactions

279   of NH_3/NH_4^+ with carbonyl functional groups (Noziere et al., 2009;Ortiz-Montalvo et

280   al., 2014;Liu et al., 2015;Qi et al., 2020). In contrast, SOA concentrations were lower

281 in the presence of NO_X, and the maximum mass concentration of toluene SOA was only

282 452 ± 18.9 μg m^{-3} with 63 ppb initial NO_X. The branching of RO_2 loss among different

283 pathways has an important influence on the product distribution and SOA formation.

284 The fate of RO_2 mainly depends on the concentrations of NO_X (Zhao et al., 2018;Liu et

285 al., 2019a;Xu et al., 2020). Several studies have shown that, instead of RO_2 reacting

286 with RO_2/HO_2, NO would react with RO_2 to form the RO intermediate and produces

287 more oxidation products with higher volatilities through fragmentation in the presence

288 of NO_X (Zhao et al., 2018;Liu et al., 2019a;Xu et al., 2020). Highly volatile compounds

289 cannot readily partition into the particle-phase, so this substantially suppresses the

290 formation of SOA.

291 The NO_X and NH_3 had opposite effects on toluene SOA formation in this study.

292 Interestingly, however, the highest SOA mass concentration (1020 ± 10.6 μg m^{-3})

293 occurred in the presence of both NO_X and NH_3, which was nearly 1.6 times higher than

294 that observed in the absence of NO_X or NH_3. Although inorganic aerosol (i.e., NH_4NO_3)

295 was formed from the interaction of NH_3 and NO_X in the chamber, the upper limit of the

296 inorganic matter only accounted for 6.6% of the total mass of particulate matter (Table

297 S1) in the $NH_3 + NO_X$ experiment. Therefore, NH_4NO_3 was not the main cause of the

298 increase in particulate matter; the co-occurrence of NH_3 and NO_X had a synergistic

299 effect on the SOA formation, because their combined effect on SOA formation was

300 greater than the sum of their separate effects. Qi et al. (2020) found that the promotion

301 of NH_3 on toluene SOA formation was more obviously under high NO_X concentration,

302 SOA yield increased 3.7% and 4.6% for 70 ppb and 160 ppb initial NO_X concentration,

303 respectively, when 200 ppb NH_3 was added into the chamber. Li et al. (2018) showed

304 that the presence NH_3 can promote the particle size growth of SOA; at the same time,

305 this particle growth rate was higher under low VOC/NO_X (or high NO_X) conditions. All

306 in all, the joint effect of multiple environmental factors on SOA formation is not the

307 simple summation of the influences of various factors on SOA formation. This may at

308 least partly explain why predictions of SOA concentrations in large-scale atmospheric

309 models, which typically describe SOA formation from data derived from chamber

310 experiments, are frequently lower than field observations (Volkamer et al., 2006).

3.2 SOA chemical composition

312 The traditional SOA formation mechanism is based on the chemical compositions

313 obtained through off-line detection of the chemical composition of SOA (Jang et al.,

314 2002;Liu et al., 2019a;Xu et al., 2020). SOA is continually evolving in the atmosphere

315 and the ageing process of SOA co-occurs with its formation process, resulting in the

316 transformation of SOA chemical composition continuously proceeding during the

317 photooxidation process. Therefore, the AMS was used for on-line measurement of the

318 SOA chemical composition and how the chemical composition evolved in the

319 photooxidation process will be discussed in the following section.

320 Chemical composition of SOA is very complex. The average carbon oxidation

321 state (OS_C) has been shown to be an ideal conceptual framework to describe changes

322 in the degree of oxidation undergone by SOA (Kroll et al., 2011), and has been widely

323 applied in field and laboratory studies (Chen et al., 2018;Mandariya et al., 2019).

324   Average OS_C calculation was shown in Supporting Information. Fig. 2 shows the

325   changes in the OS_C of toluene SOA formed in different experiments. Notably, toluene

326   SOA OS_C values was in the range between -0.5 and 0, which is consistent with that of

327   semi-volatile oxygenated organic aerosols (SV-OOA). However, the different OS_C

328   values and the change trends observed for the toluene SOA formed in different

329   conditions (with and without NH_3/NO_X) in Fig. 2 indicated that there was a

330   photooxidation mechanism active during SOA formation, which ultimately changed the

331   SOA chemical compositions.

332   The OS_C increased over time for all SOAs that were formed in the absence of NH_3.

333   There are several possible reasons for the increasing trend of OS_C values. Firstly, a

334   dynamic equilibrium of semi-volatile vapors may have been achieved between the

335   particle-phase and gas-phase during the earlier toluene oxidation process. The increase

336   of SOA led to a reduction in the concentration of gas-phase semi-volatile organic

337   products. A decreasing concentration of gas-phase semi-volatile organic compound

338   products would suppress their transformation from gas-phase to particulate-phase.

339   More lower volatility gas-phase oxidation products with higher OS_C values would then

340   be shifted to the particle phase, which would be responsible for the continuing increase

341   of SOA and its OSc. Secondly, the formed SOA could have further been oxidized by

342   OH radical through heterogeneous reactions (Kourtchev et al., 2015;Liu et al., 2019b).

343   This could be the main reason for the increase in the OS_C when the SOA concentration

344   was no longer increasing. Finally, as pointed by Malecha and Nizkorodov (2016), even

345   if there was no OH radical in the chamber, the photodegradation of SOA can produce

346   small oxygenated volatile organic compounds (e.g. acetaldehyde $OS_C=-1$, and acetone

347     $OS_C \approx -1.3$) under UV light irradiation. The photoproduction of OVOCs from SOA had

348   a lower OS_C value than that of SOA. Although the loss of SOA through

349   photodegradation is small, the OS_C value of SOA still had increased to a certain extent

350   (Malecha and Nizkorodov, 2016).

351   The fact that additional photochemical processing results in the dynamic evolution

352   of the OS_C over time has been demonstrated in both field and laboratory experiments

353   (Jimenez et al., 2009). The atmospheric oxidation of OA tends towards higher OS_C

354   regardless of the original OA source (Herndon et al., 2008). However, when NH_3 was

355   present, the OS_C of total SOA was almost unchanged for the whole photooxidation

356   period. Carboxyl and carbonyl are the main oxygen-containing functional groups

357   responsible for the toluene photooxidation production (Ji et al., 2017). An organic

358   ammonium salt with four H atoms can offset an increase in OS_C value caused by the

359   formation of organic acids/carboxy group with two O atoms through acid-base reactions

360   (Kuwata and Martin, 2012;Liu et al., 2015). In addition, NH_3/NH_4^+ may react with

361   carbonyl functional groups through Maillard reactions, consuming the oxygen atom in

362   the carbonyl group and leading to the formation of species with covalent carbon-

363   nitrogen bonds (Lee et al., 2013;Zhang et al., 2015a;Qi et al., 2020). Xu et al. (2018)

364   showed that imidazole compounds ($OS_C \approx -1.3$) generated through heterogeneous

365   reaction between NH_3 and carbonyl compounds might contribute to the decrease in the

366   OS_C of SOA. It is clear that an increase in OS_C caused by the formation of oxygen-

367   containing functional groups (e.g., carboxyl, carbonyl, etc.) would be counteracted

368 through acid-base reactions or Maillard reactions in the presence of NH_3. After 60 min

369 of UV light irradiation, there was no more SOA formation; however, the OS_C did

370 decrease slightly in Exp.2 and 3, illustrating that the NH_3 could continue to react with

371 SOA through heterogeneous processes. Huang et al. (2016) also pointed out that the

372 portion of semi-volatile products with low OS_C formed at the later stage of

373 photooxidation also contributed to the decreased OS_C.

374   The OS_C of the toluene SOA formed with NO_X was lower than that formed in the

375 absence of NO_X, no matter whether NH_3 was present in the chamber or not. This

376 indicated that an increased NO_X concentration benefits the formation of high volatility

377 oxidation products with lower OS_C values (Kroll et al., 2011;Jimenez et al., 2009).

378 However, the relationships between OS_C and SOA mass concentration with and without

379 NH_3 were the opposite to each other. Predictably, the SOA formation mechanism in the

380 presence of NO_X is different from that with $NO_X + NH_3$. In the absence of NH_3, the RO

381 intermediate, which is easily fragmented to produce relatively high-volatility

382 compounds, was the dominant product of the $NO_X + RO_2$ reaction (Zhao et al., 2018;Liu

383 et al., 2019a;Xu et al., 2020). Highly volatile compounds cannot readily partition into

384 the particle-phase, which subsequently results in a lower SOA yield in the presence of

385 NO_X (Yang et al., 2020). Thereby, both OS_C and the SOA mass concentration were

386 lower when 60 ppb NO_X was added into the chamber. However, when both NO_X and

387 NH_3 were present, the toluene derived SOA had the lowest OS_C value, but the highest

388 mass concentration. This result suggested that although NO_X promotes the formation

389 of higher volatility compounds, these higher volatility compounds (e.g. glyoxal) can

390   react with NH_3 and partition into the particle-phase, which could contribute to the

391   increase in SOA formation. Huffman et al. (2009) observed that aerosol volatility was

392   inversely correlated with the extent of oxidation of OA components. The low value of

393   OS_C in the presence of NO_X indicated that NO_X would promote the formation of the

394   relatively high-volatility compounds. However, the lower OS_C value in the presence of

395   NH_3 indicated that the high-volatility compounds would promote partitioning into the

396   particle-phase when reacting with NH_3.

397   Fragments derived from the AMS data have also been widely used to explore the

398   bulk compositions and properties of SOA (Ng et al., 2010;Ng et al., 2017). The m/z 43

399   (f43) frequency was dominated by ion $C_2H_3O^+$, which is the tracer for organic

400   compounds with alcohol and carbonyl functional groups (Alfarra et al., 2006).

401   Meanwhile, the m/z 44 (f44) signal was dominated by CO_2^+ ions, which is the tracer

402   for organic compounds with carboxyl functional groups and an indicator of highly

403   oxygenated organic aerosols (Ng et al., 2010). Here, we use the approach of Ng et al.

404   (2010) by plotting the fractions of the total organic signal at m/z 43 *vs.* m/z 44 (f43 *vs.*

405   f44). The change of f43 *vs.* f44, which has an inflection point during the photooxidation

406   process, is shown in Fig. 3 and Fig. S3. In our study, the change before the inflection

407   point was defined as the formation stage, and the linear fit of f43 *vs.* f44 for the

408   formation stage is shown by the dashed lines. The change in f43 *vs.* f44 after the

409   inflection point was defined as the stable stage, and the linear fit of f43 *vs.* f44 in this

410   stage is shown by the solid lines. The formation and stable stages of the f43 *vs.* f44

411   relationship during the experiment are discussed separately here.

412   In the stable stage, the increase in f44 and decrease in f43 with increasing OH

413   exposure indicated that the carbonyl groups in toluene SOA were oxidized to carboxyl

414   groups by the ageing process. For the experiments without NH_3 and NO_X, the slope

415   ratio of f43 *vs.* f44 was -3.9. When there was 60 ppb initial NO_X, the f43 was almost

416   stable while the f44 increased with the oxidation process. There was a lower slope ratio

417   of f43 *vs.* f44, indicating that organic compounds with more alcohol and carbonyl

418   functional groups had formed in the presence of NO_X. But for the experiments with 200

419   ppb initial NH_3, the slope ratios of f43 *vs.* f44 were only -1.1 and -1.3 in the presence

420   and absence of NO_X, respectively. According to the above results, we can see that more

421   carbonyl groups are consumed as carboxyl groups are formed in the presence of NH_3.

422   The carbonyls can be oxidized to organic acids (Kawamura and Bikkina, 2016), but

423   unreacted carbonyl can be nucleophilically attacked by NH_3/NH_4^+ to form nitrogen-

424   heterocyclic compounds, e.g., imidazole (Grace et al., 2019;Lian et al., 2020).

425   Meanwhile, the peak f44 value decreased from 0.13 to 0.10 when NH_3 was added into

426   the chamber. This suggested that the heterogeneous reaction of NH_3/NH_4^+ could

427   promote the consumption of particle-phase carbonyl groups (Xu et al., 2018), and must

428   inhibit the formation of carboxyl groups in the SOA ageing process. According to the

429   changing trend of SOA concentration over time, the photooxidation process was

430   divided into formation stage and stable stage. As shown in Fig. 1, the first half hour of

431   photooxidation when SOA concentration increased linearly with time was defined as

432   SOA formation stage. After 60 min of photooxidation, SOA concentration was not

433   changed with reaction time, and it was defined as stable stage. The differences in spectra

434   of toluene SOA in the formation stage and stable stage are shown in Fig. 4. A lower

435   signal intensity variation of CO_2^+ in the presence of NH_3 also illustrated that NH_3 would

436   inhibit heterogeneous reactions that form carboxyl groups.

437   In the formation stage, the slope ratios of f43 *vs.* f44 were almost the same for both

438   experiments without NO_X. It can thus be seen that the presence or absence of NH_3 does

439   not affect the change trend of f43 *vs.* f44 in the SOA formation stage. Therefore, the

440   gas-phase homogeneous reaction of NH_3 on SOA formation is not important. Clearly,

441   the particle-phase heterogeneous reaction was the main reaction pathway by which NH_3

442   participated in the photooxidation process and toluene SOA formation. However,

443   negative correlations were observed between f43 and f44 in the presence of NO_X. Based

444   on this, we concluded that NO_X not only affects the SOA formation through the particle-

445   phase heterogeneous reactions, but also through gas-phase homogeneous reactions.

446   **3.3 PMF results**

447   A temporal evaluation of the toluene SOA chemical composition during

448   photooxidation is vital to the analysis of the NOA formation mechanism in the presence

449   of NH_3 and/or NO_X. Therefore, this study further compared the chemical properties of

450   the SOA generated under different experimental conditions by applying a PMF analysis

451   to the HR-ToF-AMS data (Chen et al., 2019). A summary of the PMF results is

452   presented in Fig. S4-S7. For the toluene OH-photooxidation experiments with NH_3

453   and/or NO_X presence, two factors were identified from the PMF analysis in the same

454   way of Chen et al. (2019). The H/C, O/C, and N/C values of these two factors are shown

455 in Fig. 5. The factor with higher N/C values was defined as high-nitrogen OA (Hi-NOA).

456 In contrast, the factor with lower N/C values was defined as low-nitrogen OA (Lo-

457 NOA). Fig. 6 exhibits the evolution of Hi-NOA and Lo-NOA during the photooxidation

458 process as resolved from the PMF analysis of different initial NO_X/NH_3 concentrations.

459 While similar evolutionary trends were observed under different conditions, the relative

460 intensities and the chemical compositions of these two factors in each experiment were

461 not consistent.

462 For the toluene SOA formed under NH_3 conditions, both Lo-NOA and Hi-NOA

463 had similar O/C values, which were fully oxygenated with an average of 0.74 ± 0.04

464 (Fig. 5a). These O/C values were comparable to the low-volatility oxygenated organic

465 aerosols (LV-OOA) with an O/C value ranging from 0.6 to 1 (Jimenez et al., 2009). The

466 main difference between these two OA sources was the N/C ratio. The N/C ratio of Hi-

467 NOA (N/C = 0.032) was about three times higher than that of Lo-NOA (N/C = 0.010)

468 (Fig. 5a). The evolution of these two OA sources during the photooxidation process is

469 shown in Fig. 6a. The components of toluene SOA were mostly Lo-NOA during the

470 initial phase of SOA formation, but Hi-NOA toluene SOA started forming after 10

471 minutes and continued to increase. The Lo-NOA reached the maximum mass

472 concentration after 30 min of the photooxidation, and then decreased. Such a declining

473 trend of Lo-NOA at longer reaction times reflected the conversion of Lo-NOA into

474 something else in the particle-phase. As the Lo-NOA decreased, the mass concentration

475 of Hi-NOA gradually increased. Thus, the Hi-NOA should be derived from the

476 heterogeneous reaction of Lo-NOA with NH_3/NH_4^+. At the same time, it was proved

that the formation pathway of Hi-NOA was not through reaction of NH_3 with later-generation gas-phase products in the homogeneous gas phase. With the gradual replacement of Lo-NOA by Hi-NOA, the ratio of [Hi-NOA]/[Lo-NOA] stabilized at 5~6.

For the toluene SOA formed under NO_X conditions, there was not a large difference between the N/C ratios of Hi-NOA (N/C = 0.019) and Lo-NOA (N/C = 0.014) (Fig. 5c). At the end of the NO_X experiment, the ratio of [Hi-NOA]/[Lo-NOA] was only 3:2 (Fig. 6c). It follows that the contribution of the heterogeneous NO_X reaction to the N/C ratio of toluene SOA was not obvious. Therefore, the formation of NOA in the presence of NO_X mainly occurred through gas-phase homogeneous reactions, which was consistent with the results in section 3.3.

The changing trend of N/C with time in the presence of NH_3 was different to that with NO_X present. The evolutions of the N/C of SOA in different experiments are shown in Fig. 7. In the presence of NH_3, the N/C value gradually increased throughout the photooxidation process. The increased N/C value in the photooxidation process was attributed to the heterogeneous NH_3 reaction with SOA. But in the presence of NO_X, the N/C increased rapidly to its maximum value where it was stable for the rest of the reaction. This could mean that the heterogeneous reaction of toluene SOA with NO_X to form NOA was not as important as the gas-phase homogeneous reaction.

When both NO_X and NH_3 were added into the chamber, the N/C ratios of Hi-NOA and Lo-NOA were 0.062 and 0.029, respectively (Fig. 5b). The N/C ratio of Hi-NOA,

498 which was comparable to the recently isolated nitrogen-enriched OA value (0.053)

499 observed by Sun et al. (2011), was much higher than that observed in the experiments

500 with only NH_3 or NO_X. It was even higher than the sum of the N/C ratios from both

501 Exp. 2 with NH_3 and Exp. 4 with NO_X. In order to calculate the relative contributions

502 of NH_3 and NO_X to N/C, it was assumed that the effects of NH_3 or NO_X on the N/C

503 ratio in the Hi-NOA and Lo-NOA factors did not change among different experimental

504 conditions. For Lo-NOA, the contributions of NH_3 and NO_X to the N/C value were

505 0.0126 and 0.0164, and their relative intensities were 43% and 57%, respectively. While

506 for the Hi-NOA, the contributions of NH_3 and NO_X to the N/C values were 0.0404 and

507 0.0216, and their relative intensities were 65% and 35%, respectively. For the

508 experiment with both NH_3 and NO_X, the contribution of NH_3 to N/C was higher by 26%,

509 and the contribution of NO_X to N/C was higher by 17% compared to the experiments

510 with the single pollutants. The co-existence of NH_3 and NO_X further enhanced the N/C

511 value of toluene SOA, indicating that a synergetic interaction between NH_3 and NO_X

512 further enhanced organic nitrogen formation.

513 **3.4 Optical absorption**

514   The optical characteristics of toluene SOA formed from different NH_3 and NO_X

515 conditions were investigated. The MAC of toluene derived SOA detected over the range

516 of 230–600 nm is displayed in Fig. 8. Over the entire UV detection range, an increase

517 in light absorption was observed when the toluene SOA formed in the presence of NO_X

518 or NH_3.

519   By looking at Fig. 8 in detail, one can see that the MAC of toluene SOA formed

520   with (red line) and without (black line) NH_3 overlapped at 250 nm, but when the UV

521   wavelength exceeded 250 nm the MAC of the toluene SOA formed in the presence of

522   NH_3 was higher. The red line reflects an obvious characteristic absorption peak at

523   270~280 nm, which was mainly due to the absorption of the $n{\rightarrow}\pi^*$ electronic

524   transitions. The imidazole compounds were formed through the Maillard reactions

525   between NH_3/NH_4^+ with carbonyl functional groups (Zhang et al., 2015a). The C=N

526   double bonds in the organonitrogen imidazole compounds can act as effective

527   chromophores since both $\pi{\rightarrow}\pi^*$ and $n{\rightarrow}\pi^*$ transitions are chromatically active

528   (Nguyen et al., 2013). The UV/visible spectrum of imine and pyrrole show broad bands

529   at 270 nm (NIST, 2020), which was consistent with the UV absorption peak of the

530    $n{\rightarrow}\pi^*$ band observed here. According to the AMS results, carbonyl was the main

531   functional group of toluene SOA. The emergence of absorption peaks at 270~280 nm

532   demonstrated that some organonitrogen imidazole compounds (e.g. imines and pyrrole)

533   were formed through the heterogeneous reaction of toluene with NH_3. Meanwhile, the

534   high-molecular weight nitrogen-containing organic species might have formed through

535   Maillard reactions in the particle-phase (Wang et al., 2010). This was also a reason for

536   the increase in SOA mass concentration in the presence of NH_3.

537   The green line in Fig. 8 represents the MAC value of toluene-derived SOA in the

538   presence of NO_X, which was also higher than the black line (control) throughout the

539   UV detection range. When compared with the red line, the green line had no obvious

540   characteristic peak at 280 nm, but it had higher absorbance in the range between 240

541 and 280 nm. This indicated that both NO_X and NH_3 increased the absorbance of toluene

542 SOA, while the chromophores generated from the reactions between toluene-derived

543 SOA with NH_3 or NO_X did not behave in the same way.

544   The blue line in Fig. 8 represents the absorbance of toluene SOA formed in the

545 presence of both NO_X and NH_3. The MAC of toluene SOA formed in the presence of

546 both NO_X and NH_3 was higher than the toluene SOA formed in the presence of either

547 NH_3 or NO_X. There might have been a synergetic effect between NO_X and NH_3 on the

548 absorbance of toluene SOA. Considering that the mass concentration of toluene SOA

549 formed in the presence of both NH_3 and NO_X was the highest, as described in section

550 3.1, the co-existence of NH_3 and NO_X may also result in the toluene SOA having

551 stronger light absorption and atmospheric radiative forcing. We also noted a higher

552 MAC value at 280 nm, which illustrated that the presence of NO_X could promote the

553 formation of imines and pyrrole in the photooxidation system of toluene with NH_3.

4 Conclusion

555   Here we present the results of a study in which we characterized the mass

556 concentrations, chemical compositions, and optical properties of SOA formed from the

557 photooxidation of toluene under different NH_3 and NO_X concentrations. When

558 compared with the control experiment, the SOA mass concentration data showed that

559 the formation of toluene-derived SOA was enhanced in the presence of NH_3, through

560 acid-base reactions between carboxyl groups or Maillard reactions with carbonyls, but

561 inhibited in the presence of NO_X. Meanwhile, the mass concentration of toluene SOA

562 formed in the presence of both NO_X and NH_3 was higher than those formed under either

563 NH_3 or NO_X alone. This result indicated that there was a synergistic interaction between

564 NH_3 and NO_X that further enhanced toluene-derived SOA formation. At the same time,

565 the lowest OS_C value was obtained when both NH_3 and NO_X were present. We

566 concluded that highly volatile compounds, which were formed from toluene

567 photooxidation in the presence of NO_X, could react with NH_3 to form products with

568 lower volatilities, and promoted the partitioning of these products into the particle-

569 phase.

570   Synergetic effects of NH_3 and NO_X on the formation of NOA and the optical

571 properties of SOA were also observed in this study. The heterogeneous reaction was

572 responsible for the formation of NOA in the presence of NH_3. Meanwhile, an absorption

573 peak at 270~280 nm, which is characteristic of imine and pyrrole, was observed. In

574 contrast, the formation of NOA caused by NO_X alone was mainly due to a gas phase

575 homogeneous reaction.

576   In the actual atmosphere especially in Chinese urban atmosphere, NO_X and NH_3

577 abundantly co-exist. Therefore, the findings presented here clearly show that the

578 synergetic effects of NO_X and NH_3 should not be neglected. In the meantime, our work

579 provides a scientific basis for the consideration of synergistic emission reductions of

580 NH_3 and NO_X under the compound pollution conditions, which will contribute to

581 reducing the burden of aerosols in the atmosphere. It has to be noted that the

582 concentration of reactants used for the experiments is much higher than that observed

583 in polluted areas. Although the reactant concentrations including NH_3 used in this work

are much higher than those in the real urban environment, our results are applicable for the polluted urban atmosphere. In the urban atmosphere aromatic VOCs consist of numerous species and their total concentration is much higher than a single species such as toluene. On the other hand, carboxylic acids and carbonyls in the urban polluted atmosphere can be produced from aromatics and many other species. Therefore, it is reasonable for our smog chamber experiments to use toluene as a single precursor with a concentration much higher than that in the real atmosphere. Although the mechanisms of SOA formed under high precursor concentrations is expected to be the same as that under low concentrations, the kinetics are probably different. Thus, the effect of NH_3 and NO_X on the photooxidation of toluene with lower concentrations should be checked in the further study.

Data availability

The datasets are available from https://doi.org/10.6084/m9.figshare.16910953.

Author contributions

SL and GW designed the experiment. SL, DH and YW conducted the experiments. SL, DH, YW and GW performed the data interpretation. SL and GW wrote the paper. YW, SZ, XL, CW, WD contributed to the paper with useful scientific discussions or comments.

Competing interests

The authors declare that they have no conflict of interest.

Acknowledgements

This work was financially supported by National Natural Science Foundation of China (Grant No. 42130704, 42005088); the China Postdoctoral Science Foundation (Grant No. 2019M661427); Fundamental Research Funds for the Central Universities, Director's Fund of Key Laboratory of Geographic Information Science (Ministry of Education), East China Normal University (Grant No. KLGIS2021C02); and ECNU Happiness Flower Program.

Reference

Alfarra, M. R., Paulsen, D., Gysel, M., Garforth, A. A., Dommen, J., Prevot, A. S. H., Worsnop, D. R., Baltensperger, U., and Coe, H.: A mass spectrometric study of secondary organic aerosols formed from the photooxidation of anthropogenic and biogenic precursors in a reaction chamber, Atmos. Chem. Phys., 6, 5279-5293, DOI 10.5194/acp-6-5279-2006, 2006.

Babar, Z. B., Park, J.-H., and Lim, H.-J.: Influence of NH_3 on secondary organic aerosols from the ozonolysis and photooxidation of α-pinene in a flow reactor, Atmos. Environ., 164, 71-84, 10.1016/j.atmosenv.2017.05.034, 2017.

Bates, K., Jacob, D., Li, K., Ivatt, P., Evans, M., Yan, Y., and Lin, J.: Development and evaluation of a new compact mechanism for aromatic oxidation in atmospheric models, Atmos. Chem. Phys. Discuss., 2021, 1-34, 10.5194/acp-2021-605, 2021.

Berkemeier, T., Ammann, M., Mentel, T. F., Poschl, U., and Shiraiwa, M.: Organic nitrate contribution to new particle formation and growth in secondary organic aerosols from α-pinene ozonolysis, Environ. Sci. Technol., 50, 6334-6342, 10.1021/acs.est.6b00961, 2016.

Chen, C. L., Li, L. J., Tang, P., and Cocker, D. R.: SOA formation from photooxidation of naphthalene and methylnaphthalenes with m-xylene and surrogate mixtures, Atmos. Environ., 180, 256-264, 10.1016/j.atmosenv.2018.02.051, 2018.

Chen, T. Z., Liu, Y. C., Ma, Q. X., Chu, B. W., Zhang, P., Liu, C. G., Liu, J., and He, H.: Significant source of secondary aerosol: formation from gasoline evaporative emissions in the presence of SO_2 and NH_3, Atmos. Chem. Phys., 19, 8063-8081, 10.5194/acp-19-8063-2019, 2019.

Chen, Y., and Bond, T. C.: Light absorption by organic carbon from wood combustion, Atmos. Chem. Phys., 10, 1773-1787, 10.5194/acp-10-1773-2010, 2010.

Chu, B. W., Zhang, X., Liu, Y. C., He, H., Sun, Y., Jiang, J. K., Li, J. H., and Hao, J. M.: Synergetic formation of secondary inorganic and organic aerosol: effect of SO_2 and NH_3 on particle formation and growth, Atmos. Chem. Phys., 16, 14219-14230, 10.5194/acp-16-14219-2016, 2016.

de Foy, B., Lu, Z., and Streets, D. G.: Satellite NO_2 retrievals suggest China has exceeded its NO_X reduction goals from the twelfth Five-Year Plan, Sci. Rep., 6, 35912, 10.1038/srep35912, 2016.

Draper, D. C., Farmer, D. K., Desyaterik, Y., and Fry, J. L.: A qualitative comparison of secondary organic aerosol yields and composition from ozonolysis of monoterpenes at varying concentrations of NO_2, Atmos. Chem. Phys., 15, 12267-12281, 10.5194/acp-15-12267-2015, 2015.

Erisman, J. W., and Schaap, M.: The need for ammonia abatement with respect to secondary PM reductions in Europe, Environ. Pollut., 129, 159-163, 10.1016/j.envpol.2003.08.042, 2004.

Ge, S., Wang, G., Zhang, S., Li, D., Xie, Y., Wu, C., Yuan, Q., Chen, J., and Zhang, H.: Abundant NH_3 in China enhances atmospheric HONO production by promoting the heterogeneous reaction of SO_2 with NO_2, Environ. Sci. Technol., 53, 14339-14347, 10.1021/acs.est.9b04196, 2019.

Grace, D. N., Sharp, J. R., Holappa, R. E., Lugos, E. N., Sebold, M. B., Griffith, D. R., Hendrickson, H. P., and Galloway, M. M.: Heterocyclic product formation in aqueous brown carbon systems, ACS Earth Space Chem., 3, 2472-2481, 10.1021/acsearthspacechem.9b00235, 2019.

Herndon, S. C., Onasch, T. B., Wood, E. C., Kroll, J. H., Canagaratna, M. R., Jayne, J. T., Zavala, M. A., Knighton, W. B., Mazzoleni, C., Dubey, M. K., Ulbrich, I. M., Jimenez, J. L., Seila, R., de Gouw, J. A., de Foy, B., Fast, J., Molina, L. T., Kolb, C. E., and Worsnop, D. R.: Correlation of secondary organic aerosol with odd oxygen in Mexico City, Geophys. Res. Lett., 35, Artn L15804, 10.1029/2008gl034058, 2008.

Huang, D. D., Zhang, X., Dalleska, N. F., Lignell, H., Coggon, M. M., Chan, C. M., Flagan, R. C., Seinfeld, J. H., and Chan, C. K.: A note on the effects of inorganic seed aerosol on the oxidation state of secondary organic aerosol-α-Pinene ozonolysis, J Geophys Res-Atmos, 121, 12476-12483, 10.1002/2016jd025999, 2016.

Huang, Y., Lee, S. C., Ho, K. F., Ho, S. S. H., Cao, N. Y., Cheng, Y., and Gao, Y.: Effect of ammonia on ozone-initiated formation of indoor secondary products with emissions from cleaning products, Atmos. Environ., 59, 224-231, 10.1016/j.atmosenv.2012.04.059, 2012.

Huffman, J. A., Docherty, K. S., Mohr, C., Cubison, M. J., Ulbrich, I. M., Ziemann, P. J., Onasch, T. B., and Jimenez, J. L.: Chemically-resolved volatility measurements of organic aerosol fom different sources, Environ. Sci. Technol., 43, 5351-5357, 10.1021/es803539d, 2009.

Jang, M., Czoschke, N. M., Lee, S., and Kamens, R. M.: Heterogeneous atmospheric aerosol production by acid-catalyzed particle-phase reactions, Science, 298, 814-817, 10.1126/science.1075798, 2002.

Ji, Y., Zhao, J., Terazono, H., Misawa, K., Levitt, N. P., Li, Y., Lin, Y., Peng, J., Wang, Y., Duan, L., Pan, B., Zhang, F., Feng, X., An, T., Marrero-Ortiz, W., Secrest, J., Zhang, A. L., Shibuya, K., Molina, M. J., and Zhang, R.: Reassessing the atmospheric oxidation mechanism of toluene, Proc. Natl. Acad. Sci. U. S. A., 114, 8169-8174, 10.1073/pnas.1705463114, 2017.

Jiang, X. T., Lv, C., You, B., Liu, Z. Y., Wang, X. F., and Du, L.: Joint impact of atmospheric SO_2 and NH_3 on the formation of nanoparticles from photo-oxidation of a typical biomass burning compound, Environ Sci-Nano, 7, 2532-2545, 10.1039/d0en00520g, 2020.

Jimenez, J. L., Canagaratna, M. R., Donahue, N. M., Prevot, A. S., Zhang, Q., Kroll, J. H., DeCarlo, P. F., Allan, J. D., Coe, H., Ng, N. L., Aiken, A. C., Docherty, K. S., Ulbrich, I. M., Grieshop, A. P., Robinson, A. L., Duplissy, J., Smith, J. D., Wilson, K. R., Lanz, V. A., Hueglin, C., Sun, Y. L., Tian, J., Laaksonen, A., Raatikainen, T., Rautiainen, J., Vaattovaara, P., Ehn, M., Kulmala, M., Tomlinson, J. M., Collins, D. R., Cubison, M. J., Dunlea, E. J., Huffman, J. A., Onasch, T. B., Alfarra, M. R., Williams, P. I., Bower, K., Kondo, Y., Schneider, J., Drewnick, F., Borrmann, S., Weimer, S., Demerjian, K., Salcedo, D., Cottrell, L., Griffin, R., Takami, A., Miyoshi, T., Hatakeyama, S., Shimono, A., Sun, J. Y., Zhang, Y. M., Dzepina, K., Kimmel, J. R., Sueper, D., Jayne, J. T., Herndon, S. C., Trimborn, A. M., Williams, L. R., Wood, E. C., Middlebrook, A. M., Kolb, C. E., Baltensperger, U., and Worsnop, D. R.: Evolution of organic aerosols in the atmosphere, Science, 326, 1525-1529, 10.1126/science.1180353, 2009.

Kawamura, K., and Bikkina, S.: A review of dicarboxylic acids and related compounds in atmospheric aerosols: Molecular distributions, sources and transformation, Atmos. Res., 170, 140-160, 10.1016/j.atmosres.2015.11.018, 2016.

Kourtchev, I., Doussin, J. F., Giorio, C., Mahon, B., Wilson, E. M., Maurin, N., Pangui, E., Venables, D. S., Wenger, J. C., and Kalberer, M.: Molecular composition of fresh and aged secondary organic aerosol from a mixture of biogenic volatile compounds: a high-resolution mass spectrometry study, Atmos. Chem. Phys., 15, 5683-5695, 10.5194/acp-15-5683-2015, 2015.

Krechmer, J. E., Day, D. A., and Jimenez, J. L.: Always lost but never forgotten: Gas-phase wall losses are important in all teflon environmental chambers, Environ. Sci. Technol., 54, 12890-12897, 10.1021/acs.est.0c03381, 2020.

Kroll, J. H., Donahue, N. M., Jimenez, J. L., Kessler, S. H., Canagaratna, M. R., Wilson, K. R., Altieri, K. E., Mazzoleni, L. R., Wozniak, A. S., Bluhm, H., Mysak, E. R., Smith, J. D., Kolb, C. E., and Worsnop, D. R.: Carbon oxidation state as a metric for describing the chemistry of atmospheric organic aerosol, Nat. Chem., 3, 133-139, 10.1038/nchem.948, 2011.

Kuwata, M., and Martin, S. T.: Phase of atmospheric secondary organic material affects its reactivity, Proc. Natl. Acad. Sci. U. S. A., 109, 17354-17359, 10.1073/pnas.1209071109, 2012.

Laskin, A., Laskin, J., and Nizkorodov, S. A.: Chemistry of atmospheric brown carbon, Chem. Rev., 115, 4335-4382, 10.1021/cr5006167, 2015.

Laskin, J., Laskin, A., Roach, P. J., Slysz, G. W., Anderson, G. A., Nizkorodov, S. A., Bones, D. L., and Nguyen, L. Q.: High-resolution desorption electrospray ionization mass spectrometry for chemical characterization of organic aerosols, Anal. Chem., 82, 2048-2058, 10.1021/ac902801f, 2010.

Laskin, J., Laskin, A., Nizkorodov, S. A., Roach, P., Eckert, P., Gilles, M. K., Wang, B., Lee, H. J., and Hu, Q.: Molecular selectivity of brown carbon chromophores, Environ. Sci. Technol., 48, 12047-12055, 10.1021/es503432r, 2014.

Lee, A. K., Zhao, R., Li, R., Liggio, J., Li, S. M., and Abbatt, J. P.: Formation of light absorbing organo-nitrogen species from evaporation of droplets containing glyoxal and ammonium sulfate, Environ. Sci. Technol., 47, 12819-12826, 10.1021/es402687w, 2013.

Li, K., Chen, L., White, S. J., Yu, H., Wu, X., Gao, X., Azzi, M., and Cen, K.: Smog chamber study of the role of NH_3 in new particle formation from photo-oxidation of aromatic hydrocarbons, Sci. Total Environ., 619-620, 927-937, 10.1016/j.scitotenv.2017.11.180, 2018.

Lian, X., Zhang, G., Yang, Y., Lin, Q., Fu, Y., Jiang, F., Peng, L., Hu, X., Chen, D., Wang, X., Peng, P. a., Sheng, G., and Bi, X.: Evidence for the formation of imidazole from carbonyls and reduced nitrogen species at the individual particle level in the ambient atmosphere, Environ. Sci. Tech. Let., 10.1021/acs.estlett.0c00722, 2020.

Liu, M., Huang, X., Song, Y., Xu, T., Wang, S., Wu, Z., Hu, M., Zhang, L., Zhang, Q., Pan, Y., Liu, X., and Zhu, T.: Rapid SO_2 emission reductions significantly increase tropospheric ammonia concentrations over the North China Plain, Atmos. Chem. Phys., 18, 17933-17943, 10.5194/acp-18-17933-2018, 2018.

Liu, S. J., Jia, L., Xu, Y., Tsona, N. T., Ge, S. S., and Du, L.: Photooxidation of cyclohexene in the presence of SO_2: SOA yield and chemical composition, Atmos. Chem. Phys., 17, 13329-13343, 10.5194/acp-17-13329-2017, 2017.

Liu, S. J., Jiang, X. T., Tsona, N. T., Lv, C., and Du, L.: Effects of NO_X, SO_2 and RH on the SOA formation from cyclohexene photooxidation, Chemosphere, 216, 794-804, 10.1016/j.chemosphere.2018.10.180, 2019a.

Liu, S. J., Tsona, N. T., Zhang, Q., Jia, L., Xu, Y. F., and Du, L.: Influence of relative humidity on cyclohexene SOA formation from OH photooxidation, Chemosphere, 231, 478-486, 10.1016/j.chemosphere.2019.05.131, 2019b.

Liu, S. J., Wang, Y., Wang, G., Zhang, S., Li, D., Du, L., Wu, C., Du, W., and Ge, S.: Enhancing effect of NO_2 on the formation of light-absorbing secondary organic aerosols from toluene photooxidation, Sci. Total Environ., 794, 148714, 10.1016/j.scitotenv.2021.148714, 2021.

Liu, Y. C., Liggio, J., Staebler, R., and Li, S. M.: Reactive uptake of ammonia to secondary organic aerosols: Kinetics of organonitrogen formation, Atmos. Chem. Phys., 15, 13569-13584, 10.5194/acp-15-13569-2015, 2015.

Ma, P., Zhang, P., Shu, J., Yang, B., and Zhang, H.: Characterization of secondary organic aerosol from photo-oxidation of gasoline exhaust and specific sources of major components, Environ. Pollut., 232, 65-72, 10.1016/j.envpol.2017.09.018, 2018a.

Ma, Q., Lin, X., Yang, C., Long, B., Gai, Y., and Zhang, W.: The influences of ammonia on aerosol formation in the ozonolysis of styrene: Roles of Criegee intermediate reactions, R. Soc. Open Sci., 5, 172171, 10.1098/rsos.172171, 2018b.

Malecha, K. T., and Nizkorodov, S. A.: Photodegradation of secondary organic aerosol particles as a source of small, oxygenated volatile organic compounds, Environ. Sci. Technol., 50, 9990-9997, 10.1021/acs.est.6b02313, 2016.

Mandariya, A. K., Gupta, T., and Tripathi, S. N.: Effect of aqueous-phase processing on the formation and evolution of organic aerosol (OA) under different stages of fog life cycles, Atmos. Environ., 206, 60-71, 10.1016/j.atmosenv.2019.02.047, 2019.

Middlebrook, A. M., Bahreini, R., Jimenez, J. L., and Canagaratna, M. R.: Evaluation of composition-dependent collection efficiencies for the aerodyne aerosol mass spectrometer using field data, Aerosol Sci. Tech., 46, 258-271, 10.1080/02786826.2011.620041, 2012.

Moise, T., Flores, J. M., and Rudich, Y.: Optical properties of secondary organic aerosols and their changes by chemical processes, Chem. Rev., 115, 4400-4439, 10.1021/cr5005259, 2015.

Na, K., Song, C., Switzer, C., and Cocker, D. R.: Effect of ammonia on secondary organic aerosol formation from α-pinene ozonolysis in dry and humid conditions, Environ. Sci. Technol., 41, 6096-6102, 10.1021/es061956y, 2007.

Ng, N. L., Chhabra, P. S., Chan, A. W. H., Surratt, J. D., Kroll, J. H., Kwan, A. J., McCabe, D. C., Wennberg, P. O., Sorooshian, A., Murphy, S. M., Dalleska, N. F., Flagan, R. C., and Seinfeld, J. H.: Effect of NO_X level on secondary organic aerosol (SOA) formation from the photooxidation of terpenes, Atmos. Chem. Phys., 7, 5159-5174, 10.5194/acp-7-5159-2007, 2007a.

Ng, N. L., Kroll, J. H., Chan, A. W. H., Chhabra, P. S., Flagan, R. C., and Seinfeld, J. H.: Secondary organic aerosol formation from m-xylene, toluene, and benzene, Atmos. Chem. Phys., 7, 3909-3922, 10.5194/acp-7-3909-2007, 2007b.

Ng, N. L., Canagaratna, M. R., Zhang, Q., Jimenez, J. L., Tian, J., Ulbrich, I. M., Kroll, J. H., Docherty, K. S., Chhabra, P. S., Bahreini, R., Murphy, S. M., Seinfeld, J. H., Hildebrandt, L., Donahue, N. M., DeCarlo, P. F., Lanz, V. A., Prévôt, A. S. H., Dinar, E., Rudich, Y., and Worsnop, D. R.: Organic aerosol components observed in Northern Hemispheric datasets from Aerosol Mass Spectrometry, Atmos. Chem. Phys., 10, 4625-4641, 10.5194/acp-10-4625-2010, 2010.

Ng, N. L., Brown, S. S., Archibald, A. T., Atlas, E., Cohen, R. C., Crowley, J. N., Day, D. A., Donahue, N. M., Fry, J. L., Fuchs, H., Griffin, R. J., Guzman, M. I., Herrmann, H., Hodzic, A., Iinuma, Y., Jimenez, J. L., Kiendler-Scharr, A., Lee, B. H., Luecken, D. J., Mao, J., McLaren, R., Mutzel, A., Osthoff, H. D., Ouyang, B., Picquet-Varrault, B., Platt, U., Pye, H. O. T., Rudich, Y., Schwantes, R. H., Shiraiwa, M., Stutz, J., Thornton, J. A., Tilgner, A., Williams, B. J., and Zaveri, R. A.: Nitrate radicals and biogenic volatile organic compounds: Oxidation, mechanisms, and organic aerosol, Atmos. Chem. Phys., 17, 2103-2162, 10.5194/acp-17-2103-2017, 2017.

Nguyen, T. B., Laskin, A., Laskin, J., and Nizkorodov, S. A.: Brown carbon formation from ketoaldehydes of biogenic monoterpenest, Faraday Discuss., 165, 473-494, 10.1039/c3fd00036b, 2013.

NIST: NIST Chemistry WebBook Standard Reference Database 69, https://doi.org/10.18434/T4D303, 2020.

Noziere, B., Dziedzic, P., and Cordova, A.: Products and kinetics of the liquid-phase reaction of glyoxal catalyzed by ammonium ions (NH_4^+), J. Phys. Chem. A, 113, 231-237, 10.1021/jp8078293, 2009.

Ortiz-Montalvo, D. L., Hakkinen, S. A., Schwier, A. N., Lim, Y. B., McNeill, V. F., and Turpin, B. J.: Ammonium addition (and aerosol pH) has a dramatic impact on the volatility and yield of glyoxal secondary organic aerosol, Environ. Sci. Technol., 48, 255-262, 10.1021/es4035667, 2014.

Paciga, A. L., Riipinen, I., and Pandis, S. N.: Effect of ammonia on the volatility of organic diacids, Environ. Sci. Technol., 48, 13769-13775, 10.1021/es5037805, 2014.

Pathak, R. K., Stanier, C. O., Donahue, N. M., and Pandis, S. N.: Ozonolysis of alpha-pinene at atmospherically relevant concentrations: Temperature dependence of aerosol mass fractions (yields), J Geophys Res-Atmos, 112, Artn D03201, 10.1029/2006jd007436, 2007.

Peng, C., Yang, F., Tian, M., Shi, G., Li, L., Huang, R. J., Yao, X., Luo, B., Zhai, C., and Chen, Y.: Brown carbon aerosol in two megacities in the Sichuan Basin of southwestern China: Light absorption

795   properties and implications, Sci. Total Environ., 719, 137483, 10.1016/j.scitotenv.2020.137483,
796   2020.

797 Prinn, R. G., Weiss, R. F., Miller, B. R., Huang, J., Alyea, F. N., Cunnold, D. M., Fraser, P. J., Hartley, D.
798   E., and Simmonds, P. G.: Atmospheric trends and lifetime of CH_3CCl_3 and global OH
799   concentrations, Science, 269, 187-192, 10.1126/science.269.5221.187, 1995.

800 Qi, X., Zhu, S., Zhu, C., Hu, J., Lou, S., Xu, L., Dong, J., and Cheng, P.: Smog chamber study of the
801   effects of NO_X and NH_3 on the formation of secondary organic aerosols and optical properties from
802   photo-oxidation of toluene, Sci. Total Environ., 727, 138632, 10.1016/j.scitotenv.2020.138632,
803   2020.

804 Sarrafzadeh, M., Wildt, J., Pullinen, I., Springer, M., Kleist, E., Tillmann, R., Schmitt, S. H., Wu, C.,
805   Mentel, T. F., Zhao, D. F., Hastie, D. R., and Kiendler-Scharr, A.: Impact of NO_X and OH on
806   secondary organic aerosol formation from β-pinene photooxidation, Atmos. Chem. Phys., 16,
807   11237-11248, 10.5194/acp-16-11237-2016, 2016.

808 Sun, Y. L., Zhang, Q., Schwab, J. J., Demerjian, K. L., Chen, W. N., Bae, M. S., Hung, H. M., Hogrefe,
809   O., Frank, B., Rattigan, O. V., and Lin, Y. C.: Characterization of the sources and processes of
810   organic and inorganic aerosols in New York city with a high-resolution time-of-flight aerosol mass
811   apectrometer, Atmos. Chem. Phys., 11, 1581-1602, 10.5194/acp-11-1581-2011, 2011.

812 Surratt, J. D., Murphy, S. M., Kroll, J. H., Ng, N. L., Hildebrandt, L., Sorooshian, A., Szmigielski, R.,
813   Vermeylen, R., Maenhaut, W., Claeys, M., Flagan, R. C., and Seinfeld, J. H.: Chemical composition
814   of secondary organic aerosol formed from the photooxidation of isoprene, J. Phys. Chem. A, 110,
815   9665-9690, 10.1021/jp061734m, 2006.

816 Volkamer, R., Jimenez, J. L., San Martini, F., Dzepina, K., Zhang, Q., Salcedo, D., Molina, L. T., Worsnop,
817   D. R., and Molina, M. J.: Secondary organic aerosol formation from anthropogenic air pollution:
818   Rapid and higher than expected, Geophys. Res. Lett., 33, Artn L17811, 10.1029/2006gl026899,
819   2006.

820 Vu, T. V., Shi, Z., Cheng, J., Zhang, Q., He, K., Wang, S., and Harrison, R. M.: Assessing the impact of
821   clean air action on air quality trends in Beijing using a machine learning technique, Atmos. Chem.
822   Phys., 19, 11303-11314, 10.5194/acp-19-11303-2019, 2019.

823 Wang, G., Zhang, F., Peng, J., Duan, L., Ji, Y., Marrero-Ortiz, W., Wang, J., Li, J., Wu, C., Cao, C., Wang,
824   Y., Zheng, J., Secrest, J., Li, Y., Wang, Y., Li, H., Li, N., and Zhang, R.: Particle acidity and sulfate
825   production during severe haze events in China cannot be reliably inferred by assuming a mixture of
826   inorganic salts, Atmos. Chem. Phys., 18, 10123-10132, 10.5194/acp-18-10123-2018, 2018a.

827 Wang, G. H., Zhang, R. Y., Gomez, M. E., Yang, L. X., Zamora, M. L., Hu, M., Lin, Y., Peng, J. F., Guo,
828   S., Meng, J. J., Li, J. J., Cheng, C. L., Hu, T. F., Ren, Y. Q., Wang, Y. S., Gao, J., Cao, J. J., An, Z.
829   S., Zhou, W. J., Li, G. H., Wang, J. Y., Tian, P. F., Marrero-Ortiz, W., Secrest, J., Du, Z. F., Zheng,
830   J., Shang, D. J., Zeng, L. M., Shao, M., Wang, W. G., Huang, Y., Wang, Y., Zhu, Y. J., Li, Y. X., Hu,
831   J. X., Pan, B., Cai, L., Cheng, Y. T., Ji, Y. M., Zhang, F., Rosenfeld, D., Liss, P. S., Duce, R. A.,
832   Kolb, C. E., and Molina, M. J.: Persistent sulfate formation from London Fog to Chinese haze, Proc.
833   Natl. Acad. Sci. U. S. A., 113, 13630-13635, 10.1073/pnas.1616540113, 2016.

834 Wang, R. Y., Ye, X. N., Liu, Y. X., Li, H. W., Yang, X., Chen, J. M., Gao, W., and Yin, Z.: Characteristics
835   of atmospheric ammonia and its relationship with vehicle emissions in a megacity in China, Atmos.
836   Environ., 182, 97-104, 10.1016/j.atmosenv.2018.03.047, 2018b.

837 Wang, S. W., Zhang, Q., Martin, R. V., Philip, S., Liu, F., Li, M., Jiang, X. T., and He, K. B.: Satellite
838   measurements oversee China's sulfur dioxide emission reductions from coal-fired power plants,
839   Environ. Res. Lett., 10, 114015, 10.1088/1748-9326/10/11/114015, 2015.

840 Wang, X., Gao, S., Yang, X., Chen, H., Chen, J., Zhuang, G., Surratt, J. D., Chan, M. N., and Seinfeld, J.
841   H.: Evidence for high molecular weight nitrogen-containing organic salts in urban aerosols, Environ.
842   Sci. Technol., 44, 4441-4446, 10.1021/es1001117, 2010.

843 Wang, Y., Chen, Y., Wu, Z., Shang, D., Bian, Y., Du, Z., Schmitt, S. H., Su, R., Gkatzelis, G. I., Schlag,
844   P., Hohaus, T., Voliotis, A., Lu, K., Zeng, L., Zhao, C., Alfarra, M. R., McFiggans, G., Wiedensohler,
845   A., Kiendler-Scharr, A., Zhang, Y., and Hu, M.: Mutual promotion between aerosol particle liquid

water and particulate nitrate enhancement leads to severe nitrate-dominated particulate matter pollution and low visibility, Atmos. Chem. Phys., 20, 2161-2175, 10.5194/acp-20-2161-2020, 2020.

Wu, C., Zhang, S., Wang, G., Lv, S., Li, D., Liu, L., Li, J., Liu, S., Du, W., Meng, J., Qiao, L., Zhou, M., Huang, C., and Wang, H.: Efficient heterogeneous formation of ammonium nitrate on the saline mineral particle surface in the atmosphere of east asia during dust storm periods, Environ. Sci. Technol., 54, 15622-15630, 10.1021/acs.est.0c04544, 2020.

Xia, Y., Zhao, Y., and Nielsen, C. P.: Benefits of China's efforts in gaseous pollutant control indicated by the bottom-up emissions and satellite observations 2000-2014, Atmos. Environ., 136, 43-53, 10.1016/j.atmosenv.2016.04.013, 2016.

Xie, M., Chen, X., Hays, M. D., Lewandowski, M., Offenberg, J., Kleindienst, T. E., and Holder, A. L.: Light absorption of secondary organic aerosol: Composition and contribution of nitroaromatic compounds, Environ. Sci. Technol., 51, 11607-11616, 10.1021/acs.est.7b03263, 2017.

Xu, J., Huang, M. Q., Cai, S. Y., Liao, Y. M., Hu, C. J., Zhao, W. X., Gu, X. J., and Zhang, W. J.: Chemical composition and reaction mechanisms for aged p-xylene secondary organic aerosol in the presence of ammonia, J. Chin. Chem. Soc., 65, 578-590, 10.1002/jccs.201700249, 2018.

Xu, L., Kollman, M. S., Song, C., Shilling, J. E., and Ng, N. L.: Effects of NO_X on the volatility of secondary organic aerosol from isoprene photooxidation, Environ. Sci. Technol., 48, 2253-2262, 10.1021/es404842g, 2014.

Xu, L., Moller, K. H., Crounse, J. D., Kjaergaard, H. G., and Wennberg, P. O.: New insights into the radical chemistry and product distribution in the OH-initiated oxidation of benzene, Environ. Sci. Technol., 54, 13467-13477, 10.1021/acs.est.0c04780, 2020.

Yang, W. Y., Li, J., Wang, M., Sun, Y. L., and Wang, Z. F.: A case study of investigating secondary organic aerosol formation pathways in beijing using an observation-based SOA box model, Aerosol Air Qual. Res., 18, 1606-1616, 10.4209/aaqr.2017.10.0415, 2018.

Yang, Y., Vance, M., Tou, F. Y., Tiwari, A., Liu, M., and Hochella, M. F.: Nanoparticles in road dust from impervious urban surfaces: Distribution, identification, and environmental implications, Environ Sci-Nano, 3, 534-544, 10.1039/c6en00056h, 2016.

Yang, Z., Tsona, N. T., Li, J., Wang, S., Xu, L., You, B., and Du, L.: Effects of NO_X and SO_2 on the secondary organic aerosol formation from the photooxidation of 1,3,5-trimethylbenzene: A new source of organosulfates, Environ. Pollut., 264, 114742, 10.1016/j.envpol.2020.114742, 2020.

Zhang, L., Wang, Y., Feng, C., Liang, S., Liu, Y., Du, H., and Jia, N.: Understanding the industrial NO_X and SO_2 pollutant emissions in China from sector linkage perspective, Sci. Total Environ., 770, 145242, 10.1016/j.scitotenv.2021.145242, 2021a.

Zhang, Q., Jimenez, J. L., Canagaratna, M. R., Ulbrich, I. M., Ng, N. L., Worsnop, D. R., and Sun, Y.: Understanding atmospheric organic aerosols via factor analysis of aerosol mass spectrometry: a review, Anal. Bioanal. Chem., 401, 3045-3067, 10.1007/s00216-011-5355-y, 2011.

Zhang, R., Wang, G., Guo, S., Zamora, M. L., Ying, Q., Lin, Y., Wang, W., Hu, M., and Wang, Y.: Formation of urban fine particulate matter, Chem. Rev., 115, 3803-3855, 10.1021/acs.chemrev.5b00067, 2015a.

Zhang, S., Li, D., Ge, S., Liu, S., Wu, C., Wang, Y., Chen, Y., Lv, S., Wang, F., Meng, J., and Wang, G.: Rapid sulfate formation from synergetic oxidation of SO_2 by O_3 and NO_2 under ammonia-rich conditions: Implications for the explosive growth of atmospheric $PM_{2.5}$ during haze events in China, Sci. Total Environ., 772, 144897, 10.1016/j.scitotenv.2020.144897, 2021b.

Zhang, X., Cappa, C. D., Jathar, S. H., McVay, R. C., Ensberg, J. J., Kleeman, M. J., and Seinfeld, J. H.: Influence of vapor wall loss in laboratory chambers on yields of secondary organic aerosol, Proc. Natl. Acad. Sci. U. S. A., 111, 5802-5807, 10.1073/pnas.1404727111, 2014.

Zhang, X., Schwantes, R. H., McVay, R. C., Lignell, H., Coggon, M. M., Flagan, R. C., and Seinfeld, J. H.: Vapor wall deposition in Teflon chambers, Atmos. Chem. Phys., 15, 4197-4214, 10.5194/acp-15-4197-2015, 2015b.

895 Zhao, D. F., Schmitt, S. H., Wang, M. J., Acir, I. H., Tillmann, R., Tan, Z. F., Novelli, A., Fuchs, H.,
896   Pullinen, I., Wegener, R., Rohrer, F., Wildt, J., Kiendler-Scharr, A., Wahner, A., and Mentel, T. F.:
897   Effects of NO_X and SO_2 on the secondary organic aerosol formation from photooxidation of α-
898   pinene and limonene, Atmos. Chem. Phys., 18, 1611-1628, 10.5194/acp-18-1611-2018, 2018.

899 Zou, Y., Deng, X. J., Zhu, D., Gong, D. C., Wang, H., Li, F., Tan, H. B., Deng, T., Mai, B. R., Liu, X. T.,
900   and Wang, B. G.: Characteristics of 1 year of observational data of VOCs, NO_X and O_3 at a suburban
901   site in Guangzhou, China, Atmos. Chem. Phys., 15, 6625-6636, 10.5194/acp-15-6625-2015, 2015.

902

903

Tables

Table 1. Summary of experimental conditions in this study

No.	Tol_0 (ppb)	Δ Tol (ppb)	NH_3[a] (ppb)	NO_2 (ppb)	RH (%)	SOA mass conc.[b,c] ($\mu g\ m^{-3}$)	SOA yield[b] (%)
Exp.1	664.1	551.2	-	-	25 ± 1	637 ± 14.6	28.1
Exp.2	618.7	499.4	~200	-	23 ± 1	867 ± 12.7	34.7
Exp.3	620.9	526.1	~200	62	26 ± 1	1020 ± 10.6	42.7
Exp.4	645.7	539.5	-	63	25 ± 1	452 ± 18.9	19.5

[a] The concentration of NH_3 is estimated by the amount of NH_3 added and the volume of the smog chamber. [b] SOA concentration and yield were calculated after taking into account the wall loss. [c] The reported SOA mass concentrations was the peak values after the wall loss correction.

Figures
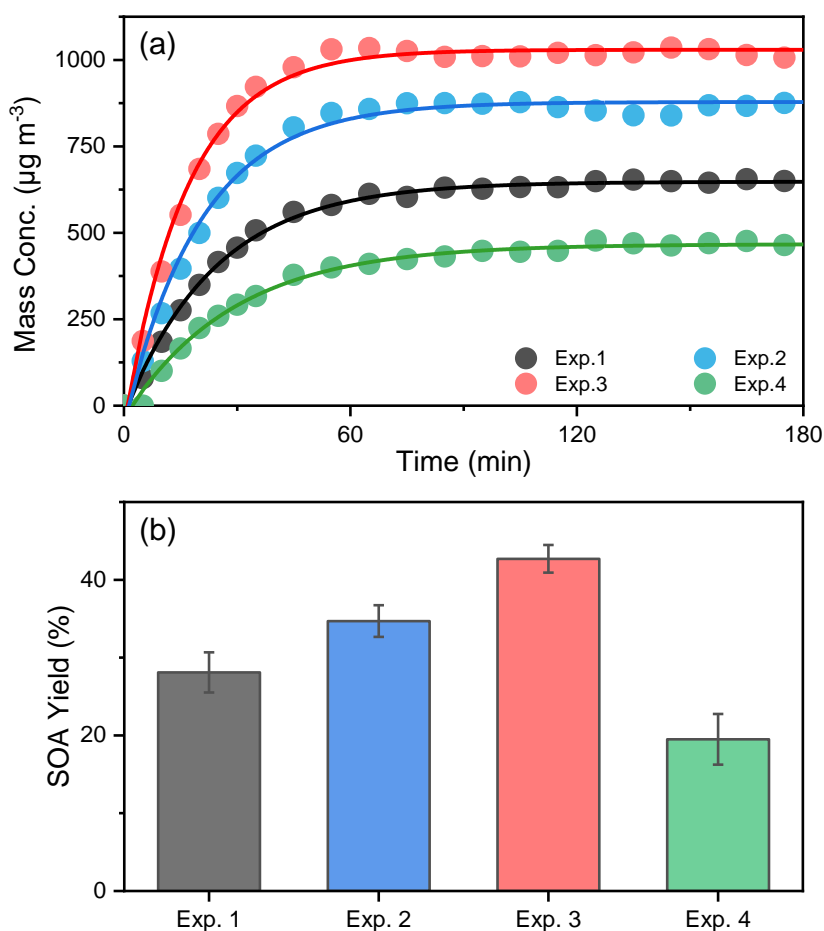
Fig. 1. The evolution of mass concentration (a) and yield (b) of toluene-derived SOA in different experiments. All the mass concentrations were wall-loss corrected. The error bars were calculated by the fluctuation of measured SOA concentration after the UV light was turn off at the end of each experiment
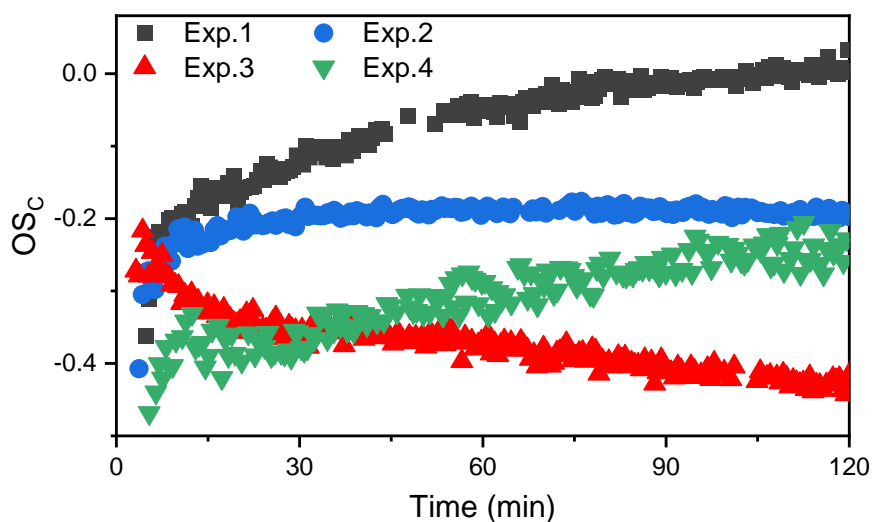
918

919 **Fig. 2.** The OS_C values for the toluene SOA formed under different NH_3/NO_X conditions.

920

921

922
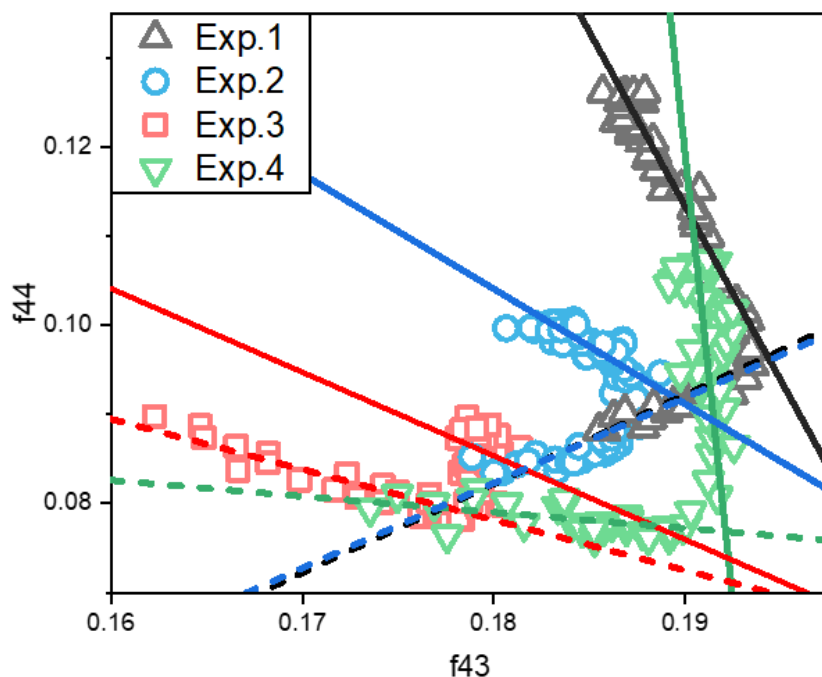
923

924 **Fig. 3.** The relationship between total organic signals at 43 m/z (f43) *vs.* 44 m/z (f44) from SOA

925 data during the photooxidation process. The f43 *vs.* f44 plots exhibited inflection points during the

926 photooxidation process. The dashed lines indicate the trends of f43 *vs.* f44 for the SOA formation

927 stage (before the inflection point) and the solid lines for the stable stage.

928
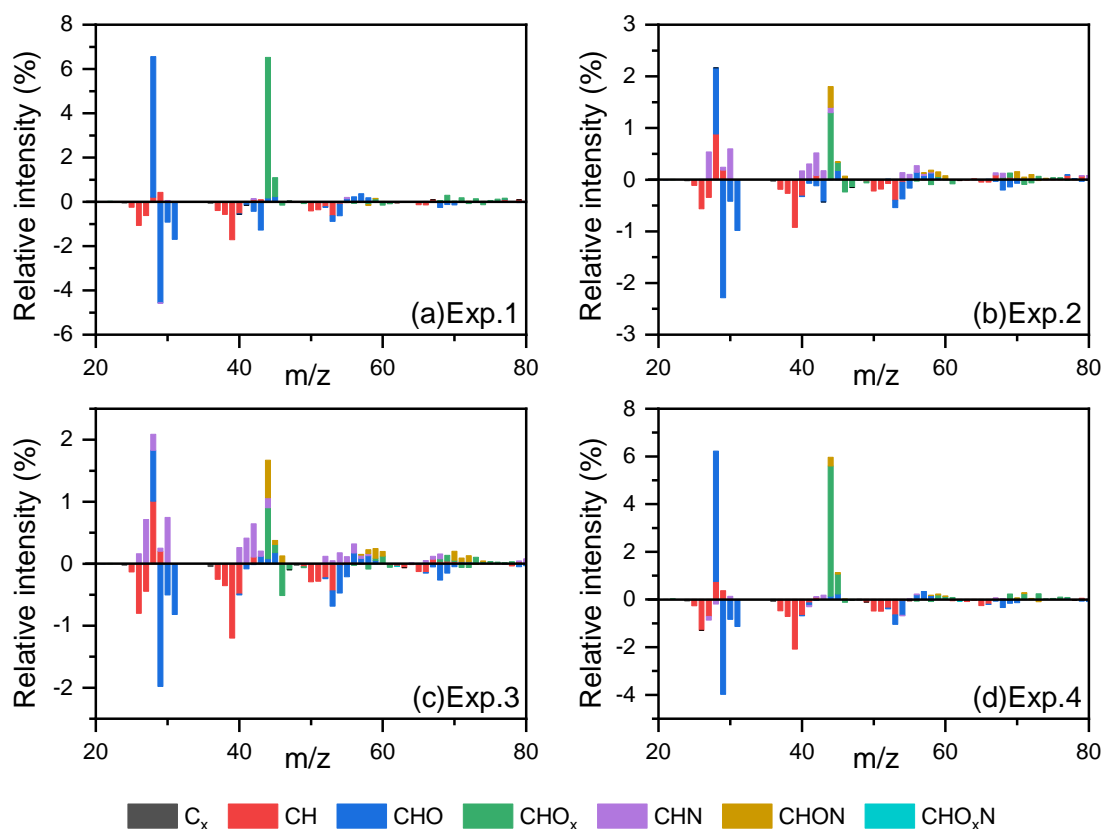
929

930 **Fig. 4.** The differential spectra of toluene SOA in the formation and stable stages. Data were taken

931 and analyzed at a high resolution but were summarized to a unit mass resolution for display. Only

932 minimal N-containing fragments could be observed in the Exp.1 without added NH_3 and NO_X.

933 These N-containing fragments could be attributed to the background NH_3 and NO_X in the chamber

934 or the systematic errors from AMS.

935

936
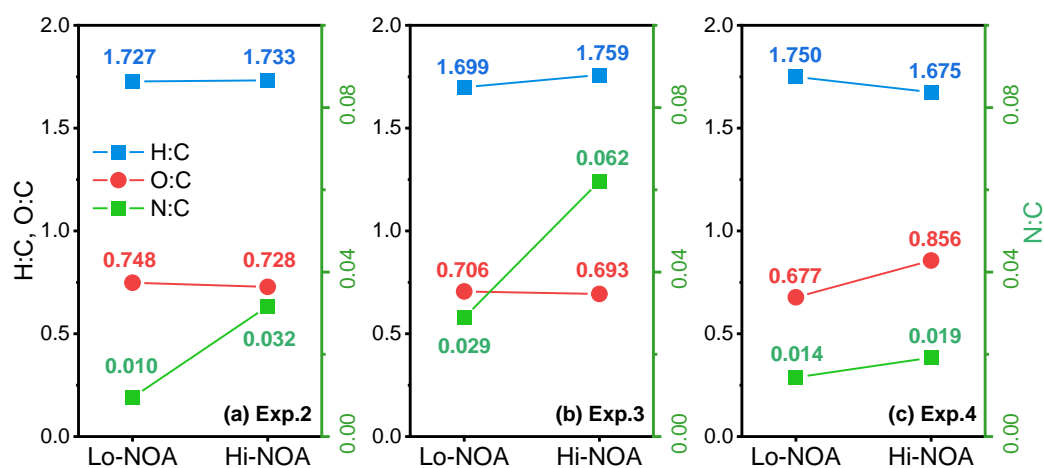
937

938 **Fig. 5.** The H/C, O/C, and N/C values of Hi-NOA and Lo-NOA for each experiment. (a) Exp. 2
939 with 200 ppb NH_3, (b) Exp. 3 with 200 ppb NH_3 and 62 ppb NO_2, and (c) Exp. 4 with 63 ppb
940 NO_2.

941

942
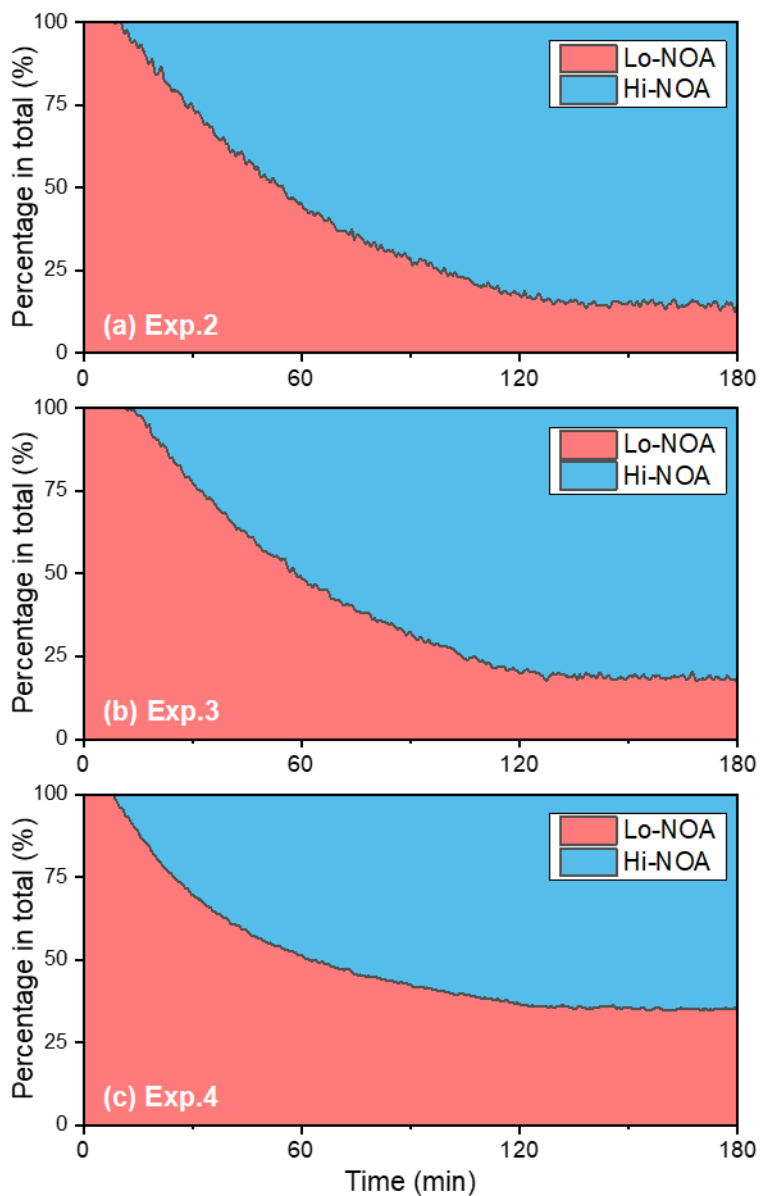
Fig. 6. The evolution of high-nitrogen OA (Hi-NOA) and low-nitrogen OA (Lo-NOA) during the
photooxidation process under different NO_X/NH_3 concentrations. Hi-NOA and Lo-NOA were not
consistent among experiments. (a) Exp. 2 with 200 ppb NH_3, (b) Exp. 3 with 200 ppb NH_3 and 62
ppb NO_2, and (c) Exp. 4 with 63 ppb NO_2.

947
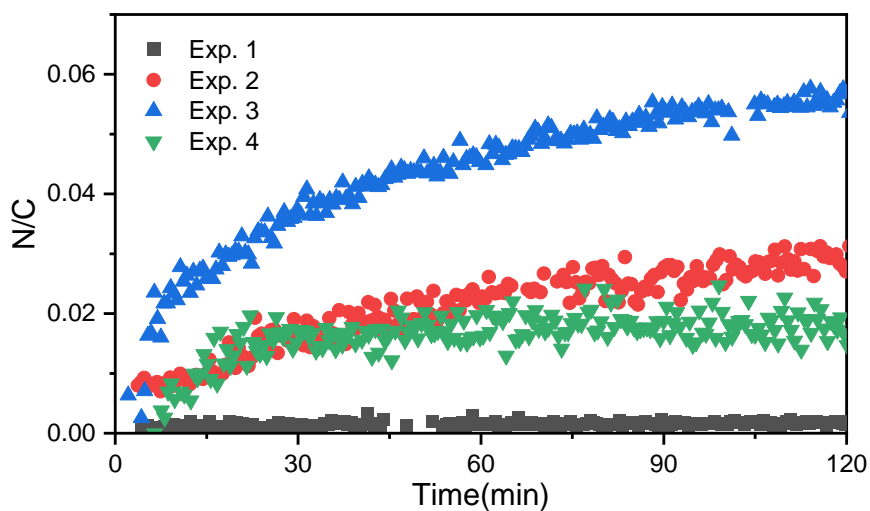
948

949 **Fig. 7.** The evolution of N/C in different experiments.

950

951

952
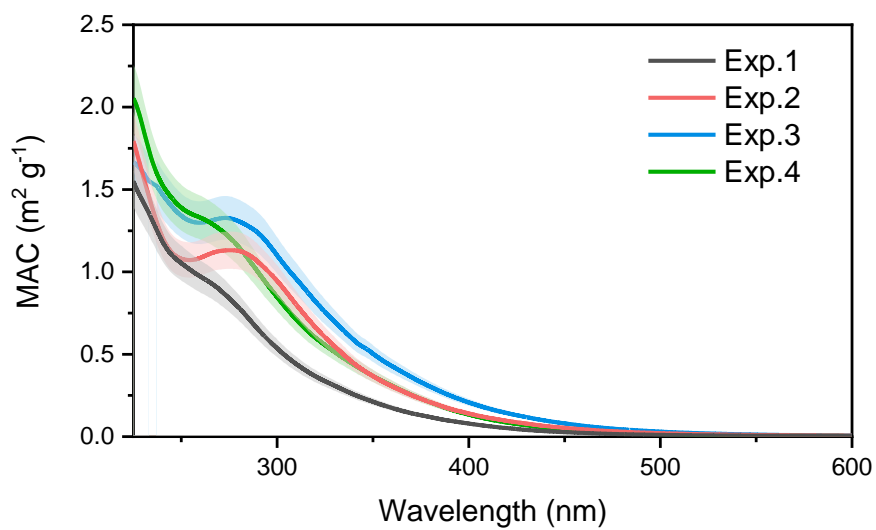
953

954 **Fig. 8.** The MAC over the range of 230 – 600 nm for the toluene SOA formed under different
955 experiment conditions.

956